Measurements of visible bremsstrahlung and automatic Bayesian inference of the effective plasma charge Z_{eff} at W7-X

A. Pavone[a] **U. Hergenhahn**[a] **M. Krychowiak**[a] **U. Hoefel**[a] **S. Kwak**[a] **J. Svensson**[a]
P. Kornejew[a] **V. Winters**[b] **R. Koenig**[a] **M. Hirsch**[a] **K.-J. Brunner**[a] **E. Pasch**[a] **J. Knauer**[a]
G. Fuchert[a] **E.R. Scott**[a] **M. Beurskens**[a] **F. Effenberg**[a,b] **D. Zhang**[a] **O. Ford**[a] **L. Vanó**[a] **R. C. Wolf**[a] **W7-X Team**[a]

[a]*Max-Planck-Institut für Plasmaphysik, Teilinstitut Greifswald, D-17491 Greifswald, DE*
[b]*University of Wisconsin-Madison, Madison, WI 53706-1609, USA*

E-mail: andrea.pavone@ipp.mpg.de

ABSTRACT: The effective charge Z_{eff} indicates the overall impurity contamination of a plasma. Z_{eff} can be derived experimentally from the intensity of the plasma bremsstrahlung emission. We describe here the diagnostic set-ups and the Bayesian modeling allowing the inference of Z_{eff} at W7-X. First results from the operational campaigns in 2017 and 2018 are shown. Measurements of the visible plasma radiation along a single line-of-sight traversing the core plasma has been carried out using a compact USB-spectrometer with a time resolution of 100 ms. A spectral region (627 - 641 nm) that is free from line emission is selected for the analysis of the bremsstrahlung emission, which also depends on electron temperature and density profiles. Electron temperature profiles are derived from either the electron cyclotron emission or the Thomson scattering diagnostic. Electron density profiles, however, have their shape information derived from Thomson scattering measurements and absolute values from single line-of-sight interferometry measurements. The Minerva framework is used to infer the profiles with Gaussian processes and develop a Bayesian model of the bremsstrahlung emission to infer line averaged Z_{eff}. The sensitivity of the diagnostic enables Z_{eff} measurements down to the lowest core electron densities observed in the last campaign of $0.75 \times 10^{19}\,\text{m}^{-3}$ with a statistical relative error of $\approx 50\%$ ($Z_{\text{eff}} = 3.2$, 100 ms integration time). The analysis is automated to routinely compute Z_{eff} after every plasma discharges.

KEYWORDS: Zeff, bremsstrahlung, Bayesian inference, neural network, Minerva

Contents

1   Introduction

In magnetically confined fusion plasmas, the study of impurity behavior is important for the assessment of plasma performance and the investigation of impurity transport [1]. The effective charge $Z_{\text{eff}} = \sum_i n_i Z_i^2 / \sum_i n_i Z_i$ is related to the concentration of impurities and indicates the overall contamination of the plasma with mainly low-Z impurities, e.g. Carbon. It is usually derived experimentally from the plasma ion-electron bremsstrahlung emission in the visible, IR or X-Ray spectral region [2–4], using an independent measurement of the electron density n_{e} and temperature T_{e}. In this work, we illustrate the diagnostic set-ups and the Bayesian modeling that allowed the inference of Z_{eff} at W7-X and we will show results from the OP1.2 experimental campaign, obtained from measurements performed with a compact USB-spectrometer. Also, we will describe the diagnostic set-up of other diagnostic systems which were routinely observing bremsstrahlung emission as well.

2   The single line-of-sight USB-spectrometer diagnostic

A compact USB-spectrometer (Red Tide USB650, Ocean Optics) collects light along a single line-of-sight that goes through the plasma core of W7-X, as shown in figure 1a. The system collects light in the visible and near infrared wavelength region, approximately from 350 to 1000 nm, as shown in figure 1b, with a time resolution of 100 ms. Due to the low light level of the calibration source only the spectral range above 450 nm can be used for the analysis. The figure also shows the bremsstrahlung emission predicted with $Z_{\text{eff}} \approx 1.5$. Details about the predictive forward model are given in the following sections. In order to infer Z_{eff} from the measured spectrum, we have selected and used a fixed wavelength window that is free of line radiation, marked with two red vertical lines in the figure, in the range of $\approx 627 - 641$ nm. The system was absolutely calibrated by measuring the diagnostic response to an Ulbricht sphere of known emissivity. The calibration has been carried out prior (pre), during (mid) and after (post) both the experimental campaigns OP1.2a and OP1.2b. The sensitivity of the diagnostic system as a function of wavelength, in units of W / (m^2 Å sr count),
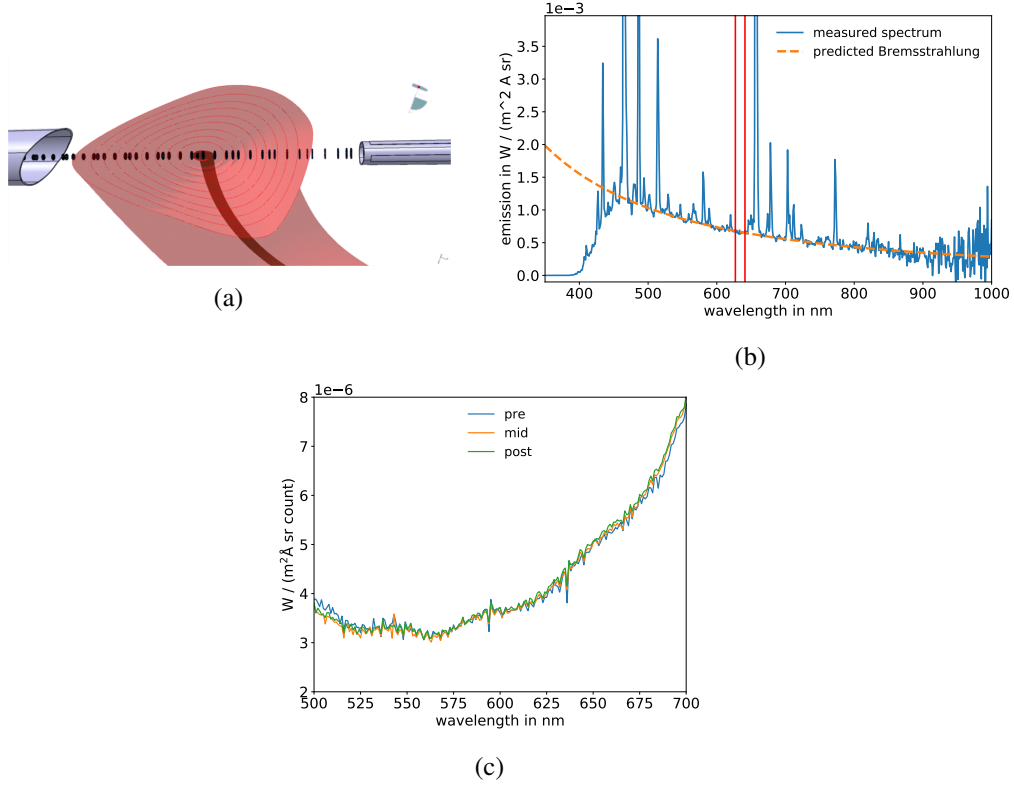
(a)

(b)

(c)

Figure 1: Figure (a) shows the single line of sight of the USB-spectrometer, the triangular W7-X plasma cross section and the magnetic axis in red. The line of sight ends in an opposite port (left hand side) thus eliminating the problem of plasma light reflections at the vessel walls. Figure (b) shows the measured spectrum of the photon flux of the plasma bremsstrahlung and line radiation (blue) as well as the predicted bremsstrahlung level with a $Z_{\text{eff}} \approx 1.5$ (dashed line). The two red vertical lines indicate the wavelength range selected and used in the analysis $\approx 627 - 641$ nm. Figure (c) shows the sensitivity spectrum of the diagnostic in the wavelength range of between 500 nm and 700 nm. Three different measurements were carried out, prior (pre), during (mid) and after (post) the experimental campaign OP1.2.

is shown in figure 1c. Multiplication by this quantity converts the measured raw data to spectral power density in absolute units (see also $1/C(\lambda)$ in equation 3.1). According to the time interval in which the data were collected, the corresponding calibration curve is applied to the data. The relative variation between the different curves is always $< 10\%$ in the wavelength range shown in the figure, indicating that the calibration remained fairly constant during the course of the campaign.

3   Bayesian modeling and inference

A model to calculate the bremsstrahlung emission is implemented in the Minerva framework [5]. The Minerva framework allows to carry out Bayesian modeling and inference in complex systems. The expected measured signal $S(\lambda)$ can be calculated from the bremsstrahlung emission at a given wavelength $V(\lambda)$ collected along the line of sight, according to equation 3.1:
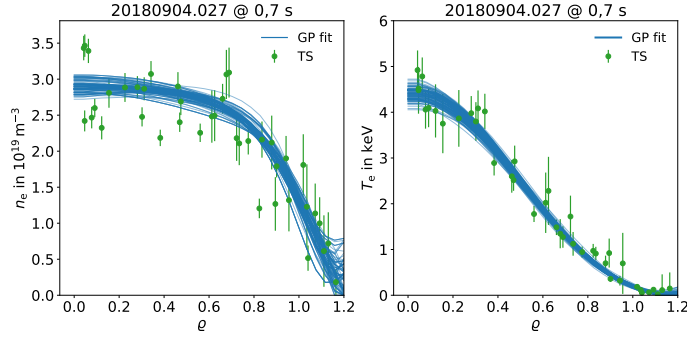
Figure 2: The electron temperature and density profiles measured by the Thomson scattering diagnostic (TS) are fitted with a Gaussian process (GP) model within the Minerva framework. The blue lines are samples from the posterior distribution found with Bayesian inference. The dots represent the measured data points together with their respective error bars.

$$S(\lambda) = C(\lambda)V(\lambda) = C(\lambda) \int g_{\text{ff}}(Z_{\text{eff}}, T_{\text{e}}, \lambda) \frac{n_{\text{e}}^2 Z_{\text{eff}}}{\sqrt{k_b T_{\text{e}}}} \exp\left(\frac{hc}{\lambda k_b T_{\text{e}}}\right) \frac{1}{\lambda^2} dl \qquad (3.1)$$

where the integration is done along the line of sight path, $g_{\text{ff}}(Z_{\text{eff}}, T_{\text{e}}, \lambda)$ is the free-free Gaunt factor modeled in Minerva according to [6], $C(\lambda)$ is an absolute calibration factor (figure 1c), and the remaining symbols are used in the conventional way referring to the respective physics constants in SI units. The single line of sight diagnostic does not allow to resolve the spatial profile of Z_{eff}, therefore, when Z_{eff} is used in the calculation of the emission along the line-of-sight, it is assumed to be constant.

According to equation 3.1, n_{e} and T_{e} are quantities required to calculate the expected emission. They are provided by a spatially resolved Thomson scattering [7] measurement and a line-integrated n_{e} measurement by the dispersion interferometer diagnostic [8], which constrains the n_{e} absolute values. Both profiles are first inferred within the Minerva framework with a Gaussian processes (GP) Bayesian model [9], where the covariance of the normal prior distributions of the profiles is modeled with a covariance function, parametrised in terms of the profile length scale. The posterior solution found is "smooth" and it is affected by the number of observed data points and their respective uncertainties, which in this case do not include systematic errors. An example case of such procedure is shown in figure 2, where the samples from the posterior distribution are shown in blue and the measured data points are labeled as TS. The coordinate on the x-axis is the effective radius $\rho = \sqrt{\psi/\psi_{\text{LCFS}}}$, where ψ is the magnetic flux and ψ_{LCFS} is the magnetic flux at the last closed flux surface.

Since the Bayesian analysis is meant to be carried automatically after every plasma discharge, a fallback solution is provided for those cases in which Thomson scattering measurements are not available. The n_{e} profile is assumed to be parabolic, and absolute values are scaled accordingly using interferometer measurements, as previously mentioned; the T_{e} profile, on the other hand, is obtained from measurements by the electron cyclotron emission (ECE) diagnostic using the cold resonance approximation [10, 11].

4 Results

Z_{eff} can be inferred by comparing predicted and measured bremsstrahlung emission signals. Two example cases from experiments 20180920.042 and 20181016.023 are depicted in figure 3a and 3b, showing discharges in which the plasma was seeded by Ne and N_2, respectively [12]. Ne was injected at 5, 7, 9 and 11 s for 200 ms, whereas N_2 was injected at 2 s for 50 ms and continuously at 3-7 s; a second valve was open at 5-7 s, increasing the gas flow rate by a factor of ≈ 2. Corresponding to the injection times, we observe an increase in the Z_{eff} values and in the total plasma radiation measured with a bolometer [13]. The Z_{eff} error bars are obtained taking into account signal statistics, the absolute calibration and the uncertainties in the n_{e} and T_{e} profiles. In the figures, the time evolution of other relevant parameter is also shown: the power from the electron cyclotron resonance heating (ECRH), the line integrated density n_e measured with the interferometer, and the value of the electron temperature in the core T_e as measured with the ECE diagnostic.

In figure 3c we show the case of a very low density discharge demonstrating the lower sensitivity limit of the diagnostic at 100 ms integration time. A line-of-sight averaged density n_{e} of 0.75 $\times 10^{19}\,\mathrm{m}^{-3}$ as measured with the interferometer at ≈ 0.5 s allowed to measure a $Z_{\mathrm{eff}} \approx 3.2$ with a statistical error of $\approx 50\%$. In the second plot from the top, the measured signal for each pixel in the considered wavelength range is show at every time point; the large noise level is clearly visible.

The Z_{eff} values inferred with the USB-spectrometer were also compared to those found with the charge exchange recombination spectroscopy (CXRS) system [14, 15] for two discharges 20180927.042 and 046 in which He was injected during the experiments and the neutral beam injection (NBI) system was active. According to a preliminary analysis, the CXRS system allowed to measure a H/He ratio of 0.3/0.7 and 0.85/0.15 in the first and second discharge respectively, and a 2% concentration of C^{6+} in the core in both experiments. From these values, the lower limit of Z_{eff} was then estimated as ≈ 2.1 and 1.7, compared to 1.9 ± 0.4 and 1.5 ± 0.3 as found with the USB-spectrometer.

5 Conclusions and future works

A compact, single line-of-sight USB-spectrometer allows to measure bremsstrahlung emission and infer Z_{eff} at the Wendelstein 7-X stellarator. The diagnostic was operating during the OP1.2 routinely providing the line-of-sight averaged Z_{eff}. A Bayesian model was implemented in the Minerva framework, allowing to infer Z_{eff} and to provide Gaussian process fits of n_{e} and T_{e} profiles combining measurements of the Thomson scattering and dispersion interferometer measurements.

In the context of future works, we want to mention that more systems dedicated for the Z_{eff} measurement are also available and collected data during the experiments, but they are not yet modeled and inference was not carried out on such measurements. Specifically, two additional detectors share the same line of sight of the USB-spectrometer. One collects light emitted in the near infrared range of 750-950 nm, with spectral resolution of ≈ 1 nm and typical time resolution of 50 ms. A second one collects visible light at 523 nm and 630 nm using interference filters with a bandwith of 2 nm, and time resolution of 100 kHz. A third system is equipped with 27 lines of sight and operate in the range 750-950 nm, and can therefore provide information to infer spatially resolved Z_{eff}. In future works we aim at modeling all these systems and adding other diagnostics
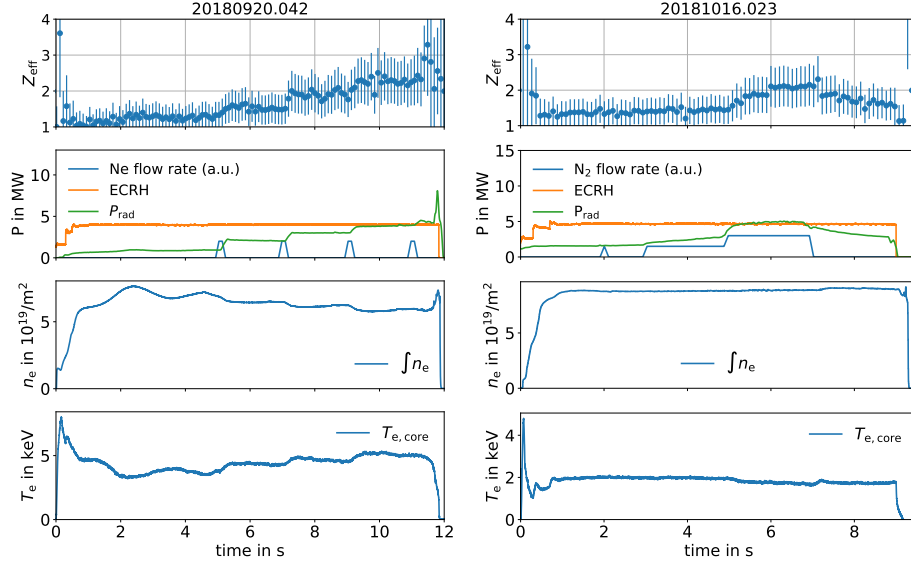
(a) A case of Ne injection.

(b) A case of N_2 injection.
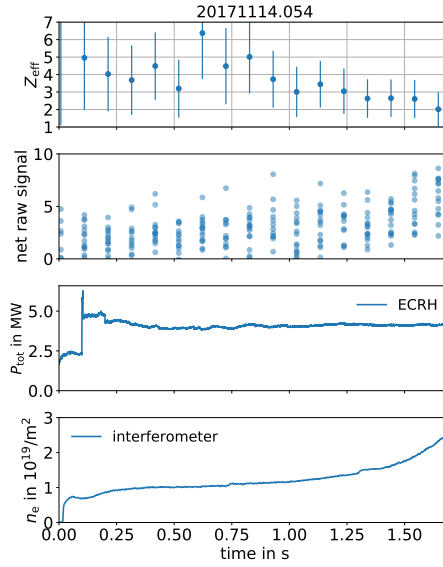
(c) A low density discharge.

Figure 3: The time evolution of Z_{eff} with respective error bars and other relevant parameters for three example cases. Figures (a) and (b) show the case of two seeding experiments, with Ne and N_2 respectively. A discrete increase in Z_{eff} and total radiated power P_{rad} is observed after each injection of seeding gas. The low density discharge in figure (c) allowed to assess the sensitivity of the diagnostic: a line-of-sight averaged density of 0.75×10^{19} m^{-3} at 0.5 s allowed to measure a $Z_{eff} \approx 3.2$ with a statistical error of $\approx 50\%$

containing information on Z_{eff} (as CXRS, X-ray spectrometers) within the Minerva framework, so to exploit all available information for the inference of Z_{eff} profiles.

Acknowledgments

References

[1] G. Verdoolaege, M. G. Von Hellermann, R. Jaspers, M. M. Ichir and G. Van Oost, *Integrated bayesian estimation of zeff in the textor tokamak from bremsstrahlung and cx impurity density measurements*, *AIP Conference Proceedings* **872** (2006) 541–548, [https://aip.scitation.org/doi/pdf/10.1063/1.2423317].

[2] M. Krychowiak, R. König, T. Klinger and R. Fischer, *Bayesian analysis of the effective charge from spectroscopic bremsstrahlung measurement in fusion plasmas*, *Journal of Applied Physics* **96** (2004) 4784–4792, [https://doi.org/10.1063/1.1787135].

[3] H. Y. Zhou, S. Morita, M. Goto and M. B. Chowdhuri, *Zeff profile measurement system with an optimized czernyturner visible spectrometer in large helical device*, *Review of Scientific Instruments* **79** (2008) 10F536, [https://doi.org/10.1063/1.2953489].

[4] H. Meister, R. Dux, L. D. Horton, B. Kurzan, H. Zohm and P. J. McCarthy, *An integrated system to measure the effective charge of fusion plasmas in the asdex upgrade tokamak*, *Review of Scientific Instruments* **74** (2003) 4625–4633, [https://doi.org/10.1063/1.1605265].

[5] J. Svensson and A. Werner, *Large Scale Bayesian Data Analysis for Nuclear Fusion Experiments*, *IEEE International Symposium on Intelligent Signal Processing* (2007) 1–6.

[6] R. S. Sutherland, *Accurate free-free Gaunt factors for astrophysical plasmas*, *Monthly Notices of the Royal Astronomical Society* **300** (1998) 321–330.

[7] S. Bozhenkov, M. Beurskens, A. D. Molin, G. Fuchert, E. Pasch, M. Stoneking et al., *The thomson scattering diagnostic at wendelstein 7-x and its performance in the first operation phase*, *Journal of Instrumentation* **12** (oct, 2017) P10004–P10004.

[8] J. Knauer, P. Kornejew, H. T. Mora, M. Hirsch, A. Werner and R. Wolf, *A new dispersion interferometer for the stellarator wendelstein 7-x*, in *43 rd European Physical Society Conference on Plasma Physics, Leuven, Belgium P*, vol. 4, 2016.

[9] C. E. Rasmussen and C. K. I. Williams, *Gaussian Processes for Machine Learning*. The MIT Press, 2006.

[10] M. Hirsch, U. Höfel et al., *Ece diagnostic for the initial operation of wendelstein 7-x*, *EPJ Web Conf.* **203** (2019) 03007.

[11] U. Hoefel, M. Hirsch, S. Kwak, A. Pavone, J. Svensson, T. Stange et al., *Bayesian modeling of microwave radiometer calibration on the example of the wendelstein 7-x electron cyclotron emission*

diagnostic, *Review of Scientific Instruments* **90** (2019) 043502,
[https://doi.org/10.1063/1.5082542].

[12] F. Effenberg et al., *First demonstration of radiative power exhaust with impurity seeding in the island divertor at wendelstein 7-x*, *Nuclear Fusion* (2019) forthcoming.

[13] D. Zhang, R. Burhenn, R. Koenig, L. Giannone, P. A. Grodzki, B. Klein et al., *Design criteria of the bolometer diagnostic for steady-state operation of the w7-x stellarator*, *Review of Scientific Instruments* **81** (2010) 10E134, [https://doi.org/10.1063/1.3483194].

[14] O. Ford and other, *Charge exchange recombination spectroscopy at wendelstein 7-x*, *Review of Scientific Instruments* (2019) forthcoming.

[15] L. Vanó and other, *Studies on carbon content and transport with charge exchange spectroscopy on w7-x*, *EPS Proceedings* (2019) forthcoming.